Communication

Effect of Chemistry on Nonisothermal Tempering and Softening of Dual-Phase Steels

S.S. NAYAK, V.H. BALTAZAR HERNANDEZ, and Y. ZHOU

In sequel to our recent report,[1] we demonstrate in this article the effect of chemistry on nonisothermal tempering and softening behavior of dual-phase steels. The martensite morphology and tempered structure were analyzed using electron microscopy. Electron energy loss spectrometry and energy-dispersive X-ray spectroscopy were used for a compositional analysis. It was observed that characteristic of the tempered structure in dual-phase (DP) steels was a function of prior martensite structure and chemistry, which in turn influence the extent of softening.

DOI: 10.1007/s11661-011-0868-8

An important issue with DP steel, which hampers its use in practical applications, is heat-affected zone (HAZ) softening that occurs in welding because of the tempering of the martensite phase in the base metal (BM).[2–8] Tempering of martensite is well documented in the literature, but it has been addressed mostly to fully martensitic steels subjected to isothermal tempering treatment.[9–11] In the context of explaining the tempering of martensite that causes softening in DP steel, we recently compared the characteristics of martensite tempering in DP steels subjected to isothermal and nonisothermal tempering, and the consequent effect on softening behavior.[1] Nonisothermal tempering cycle was achieved in resistance spot welding (RSW). We observed fine cementite in nonisothermally tempered DP steel unlike the coarser and spheroidized cementite in isothermal tempering. In addition, the extent of softening was observed to vary with steel chemistry and martensite structure, which likely indicates a dependence of tempering behavior on chemistry. Thus, the objective of the current article was to support our recent study by investigating the effect of chemistry on the nonisothermal tempering of martensite in DP steels and its effect on softening.

The starting materials were three zinc-coated 1.2-mm thick DP steel sheets. DP steels used in the study were designated, according to their alloying level and, in turn, carbon equivalent (CE) calculated using Yurioka formula,[12] as follows: lean (DP_L), moderate (DP_M), and rich (DP_R), which are listed in Table I. All chemistries listed are in wt pct.

The mechanical properties and volume fraction of martensite of the DP steels are also included in the table. A standard metallographic analysis was used for calculating the volume fraction (f_m). Figure 1 illustrates the nonisothermal tempering thermal cycle (RSW) used in the study; the details of this are reported elsewhere.[1,5] Figure 2 illustrates a schematic cross section of resistance spot-welded DP steel showing different zones of a weldment. It is to be noted that HAZ is subdivided at the location of Ac_1 as upper-critical and subcritical regions[5]; however, the study was focused on subcritical HAZ (location "a" in Figure 2) where maximum softening occurs in the DP steel welds[5] and BM (location "b" in Figure 2), where martensite does not get affected in nonisothermal tempering.

The microstructure of the subcritical HAZ and BM (location "a" and "b" in Figure 2, respectively) of the DP steels were analyzed using a JEOL7000F (Japan Electron Optics Ltd., Tokyo, Japan) scanning electron microscope (SEM) and a Philips CM12 (Philips, Irvine, CA) transmission electron microscope (TEM) operated at 120 kV. TEM samples of the BM were prepared by standard twin-jet electropolishing, whereas carbon extraction replicas were made for structural analysis of the precipitated carbides (at subcritical HAZ) in nonisothermally tempered specimens. Sample preparation details were reported in our recent study.[1] The compositions of carbides were examined using electron energy loss spectrometry (EELS) and TEM energy-dispersive X-ray spectroscopy (EDX). EELS analysis was conducted in a TITAN II 800-300 (FEI, Hillsboro, OR) cryo *in situ* TEM operated at 300 kV. A Shimadzu HMV-2000 (Shimadzu Corporation, Kyoto, Japan) hardness tester was used to measure Vickers microhardness using a load of 200 g with a 15-second dwell time keeping 200 μm spacing between subsequent indentations. The carbide particle size was measured using high-magnification SEM images and TEM images of extracted replicas.

Representative SEM micrographs (Figure 3(a) through (c)) illustrating the ferrite matrix (α) and martensite (α') in the BM microstructure delineated the distinct morphology of α'-phase in all the three DP steels (Table I). It may be noted that α and α' has body-centered cubic and body-centered tetragonal crystal structure, respectively. For example, the martensite blocks were defined finely in DP_L steel (Figure 3(a)), whereas a solid featureless morphology of the α' phase was observed in DP_M and DP_R steels (Figure 3(b) and (c)). A comparison of all three BM microstructures indicated a larger grain size of α' in DP_L, whereas a smaller grain size was observed in DP_M followed by DP_R steel. Bright-field images of α' and corresponding

S.S. NAYAK, Postdoctoral Fellow, and Y. ZHOU, Director and Professor, are with the Center for Advanced Materials Joining, Department of Mechanical and Mechatronics Engineering, University of Waterloo, Waterloo, Ontario N2L 3G1, Canada. Contact e-mails: sashank@uwaterloo.ca and sashank.nayak@gmail.com V.H. BALTAZAR HERNANDEZ, formerly Graduate Student, with the Department of Mechanical Engineering, University of Waterloo, is now Professor, with the MPyM-EPMM Academic Unit of Engineering, Autonomous University of Zacatecas, C.P. 98000 Zacatecas, Mexico.

Manuscript submitted April 13, 2011.
Article published online August 31, 2011

Table I. Details of the DP Steels Studied: CE was used to categorize the DP steels

Steel	DP_L	DP_M	DP_R
C	0.150	0.132	0.147
Mn	1.500	1.907	1.719
Cr	0.021	0.161	0.612
CE	0.390	0.475	0.525
f_m (pct)	54	48	40
α'-carbon content (calculated wt pct)	0.273	0.269	0.360
Hardness (VHN)	330	301	281
0.2 pct yield strength (MPa)	674	534	524
Ultimate tensile strength (MPa)	1061	979	820
Total elongation (pct)	12	15	18

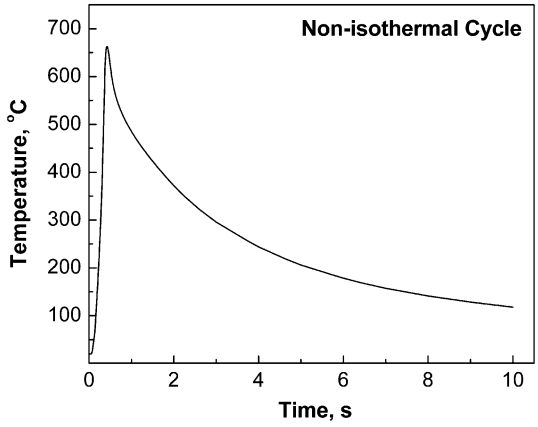

Fig. 1—Thermal cycle of nonisothermal tempering implemented on DP steels[1,5].

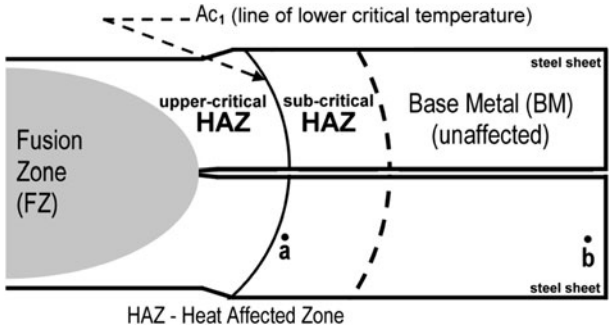

Fig. 2—Schematic cross-section of resistance spot weld showing the different zones: the fusion zone (FZ), HAZ, and BM. The HAZ is divided into upper- and subcritical HAZ[5].

selected area diffraction (SAD) patterns (insets) in all DP steels are illustrated in Figures 3(d) and (f). In accordance with SEM observation, coarser lath morphology was observed in DP_L steel (Figure 3(d)) with relatively larger blocks compared with that in the DP_M steel (Figure 3(e)) with SAD patterns confirming $[011]_{\alpha'}$ and $\left[\bar{1}11\right]_{\alpha'}$ zone axes in DP_L and DP_M steels, respectively. Interestingly, DP_R steel was observed to contain twinned plates of α' (Figure 3(f)) as confirmed by the indexed SAD pattern showing streaks of $\left(\frac{2}{3}\frac{\bar{5}}{3}\frac{5}{3}\right)$ twin reflections along with the $[011]_{\alpha'}$ zone axis. This observation was in accordance with α' carbon content: low carbon α' (DP_L = 0.273 wt pct and DP_M = 0.269 wt pct) consisted laths whereas twinned morphology was observed in high-carbon α' (DP_R = 0.360 wt pct).[9,11]

The high density of dislocations observed in the BM of DP_M steel (Figure 4(a)) was a typical characteristic feature of low-carbon martensite laths.[13] The SAD patterns shown in Figures 4(b) and (c), taken from the locations indicated by circles "b" and "c" in Figure 4(a), were indexed to contain spots from $[001]_{\alpha'}$ and $\left[\bar{1}13\right]_{\alpha}$ zone axes, respectively, confirming the presence of α'-phase and α matrix in DP_M steel. It is to be noted that TEM bright-field images of the DP_M steel BM delineated the microstructural features distinctly, *i.e.,* random arrays of dislocations in the α-matrix, α'-phase, prior-γ grain boundaries (α/α' boundaries), and block boundaries (marked by a white dotted line), which separate α'-blocks containing parallel laths.[1] It was also concluded that α'-phase in the DP_M steel has microstructural features similar to low-carbon martensitic steel.

Figure 5 illustrates representative SEM images of tempered structure and bright-field images of carbides in replicas of all nonisothermally tempered DP steels. A close observation of the tempered structures suggested a severely decomposed α' in DP_L steel (Figure 5(a)) and a broken lathy appearance in DP_M (Figure 5(b)) and DP_R steels (Figure 5(c)). Even though carbide precipitation was observed to be distributed thoroughly in all tempered martensite, coarser carbides were observed in DP_L steel, whereas finer carbides precipitated in DP_R steel. The finer carbides were associated with the higher carbon content, leading to the twinned substructure of α'-phase in DP_R steel (Figure 3(f)), which further confirms that the tempering characteristic of α' in DP steel is similar to that of martensitic steel with similar carbon content.[14] The inset SAD patterns showed spots from the [010] zone axis of orthorhombic structure corroborating precipitation of cementite (θ), irrespective of DP steel chemistry (Figure 5(d) and (f)); however, the average carbide size of cementite in nonisothermally tempered DP steels suggested a trend: DP_L (300 ± 23 nm) $\rightarrow$ DP_M (45 ± 14 nm) $\rightarrow$ DP_R (30 ± 12 nm).

Figure 6 shows a dark-field image of a cementite particle obtained, using (1) (010) diffraction spot, from nonisothermally tempered DP_M steel (Figure 6(a)); (2) EELS spectrum of the cementite indicating peaks of

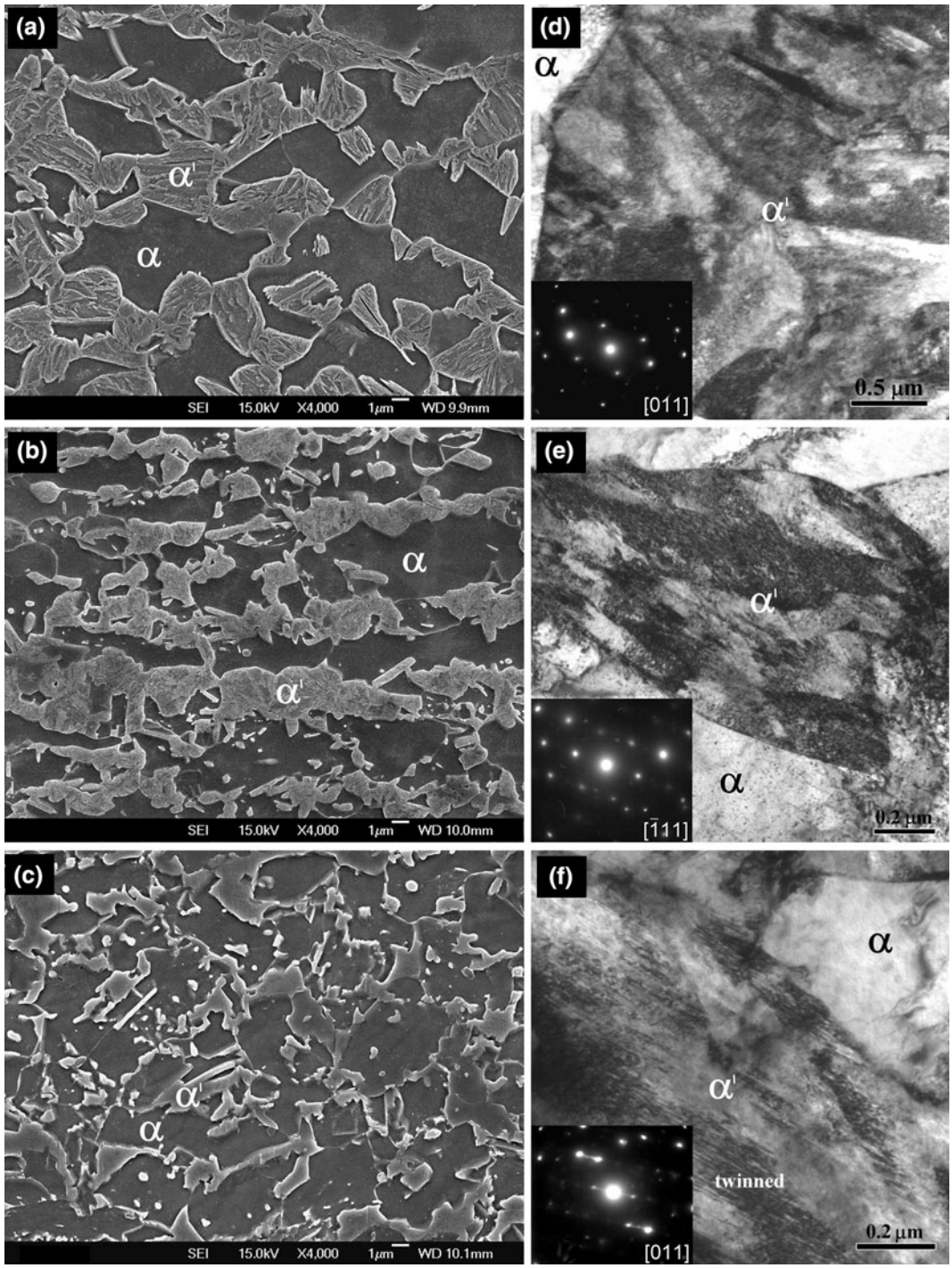

Fig. 3—SEM images showing the BM microstructure of (*a*) DP_L, (*b*) DP_M, and (*c*) DP_R steels, and the BF images of the α' phase containing the inset SAD patterns showing spots from $[011]_{\alpha'}$, $[\bar{1}11]_{\alpha'}$, and $[011]_{\alpha'}$ zone axes in (*d*) DP_L, (*e*) DP_M, and (*f*) DP_R steels taken with a camera length of 770 mm, 530 mm, and 1100 mm, respectively.

substitutional elements *viz*. Fe, Mn, and Cr (Figure 6(b)); and (3) intensity profile made across the cementite (Figure 6(c)) following the path of the electron beam (marked as spectrum image in Figure 6(a)). Quantification of the spectrum indicated a relatively larger concentration of Fe (80 wt pct) in cementite compared with Mn (16 wt pct) and Cr (4 wt pct). The distribution of alloying elements was consistent within the cementite with Fe, having a high-intensity profile confirming the EELS spectrum analysis. An EDX analysis of the cementite in all three DP steels (Figure 7) indicated characteristic peaks of only Fe in the DP_L specimen; however, additional Mn and Cr peaks were observed in the spectrums of DP_M and DP_R steels. Supporting the

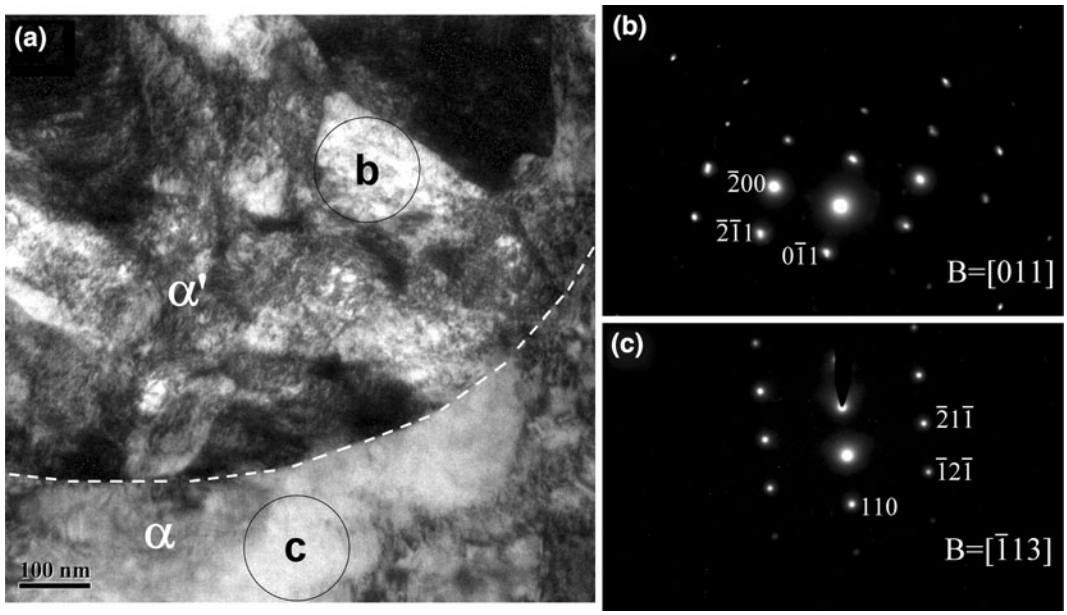

Fig. 4—(*a*) Bright-field image delineating prior γ grain boundary in BM of DP_M steel, and the corresponding SAD patterns for (*b*) α'-phase and (*c*) α-matrix confirming $[011]_{\alpha}'$ and $\left[\bar{1}13\right]_{\alpha}$ zone axes, respectively. The camera length used for the diffraction pattern was 530 mm.

EELS result, the peaks of Cr in cementite were less intense than that of Mn in DP_M steel, whereas stronger peaks of Cr were observed in the cementite of the DP_R steel. A summary of the relative percentage of substitutionals within cementite in DP_L, DP_M, and DP_R steels is listed in Table II.

An EELS and EDX analysis suggested that the substitutional composition of precipitated cementite in nonisothermal tempering reflects the substitutional level in the bulk DP steel chemistry. For example, cementite of DP_R steel comprised a high Cr and Mn content, suggesting the precipitation of substitutional rich cementite. This reflects the Cr and Mn levels available for partitioning from bulk composition (Table I). The presence of Mn and Cr substitutionals in cementite precipitated in nonisothermally tempered DP steels suggested that thermodynamically stable cementite adopts the stoichiometric form of M_3C (M = Fe, Mn, Cr), which is consistent with the previous reports.[10,14–16] In this work, nonisothermal tempering of DP_R steel resulted cementite with a stoichiometric form of $(Fe_{0.7}Mn_{0.12}Cr_{0.18})_3C$.

The stoichiometric form of cementite is derived from the concentration of alloying elements within cementite (Cr, Mn) or at the θ/α interface (Si). In this case, the alloying elements controlled the growth rate of cementite by restricting the diffusion of carbon, thus reducing the cementite coarsening.[17] Studies on composition of cementite with substitutional elements (Fe, Mn, and Cr) in isothermally tempered martensitic steels indicated that the partition of alloying elements between cementite and matrix is negligible in the temperature range of 623 K to 823 K (350 °C to 550 °C) *i.e.,* paraequilibrium state of cementite in which carbon diffusion dominates[10,11,14,16,18]; however, increasing the tempering temperature to 723 K (450 °C) resulted in enrichment of cementite with Cr and Mn.[14] A subsequent increase in tempering temperature to 923 K (650 °C) resulted in a gradual increase in Mn concentration with the enrichment strongly retarding the growth of cementite.[10] A similar effect was observed with Cr addition.[11] In the current study, the substitutional content in the precipitated cementite was related to the richness of steel chemistry, which suggested a restriction in diffusion of carbon even at high temperature, *i.e.,* 923 K (650 °C), which was further supported by insufficient time available for diffusion of carbon into cementite in nonisothermal tempering of DP steels because of rapid heating in nonisothermal tempering.[1] Thus, considering the cementite size and compositional analysis, it was concluded that cementite precipitation in the DP_L steel was controlled by diffusion of carbon because the cementite composition (Table II) is near to the bulk steel chemistry (Table I). In addition, it is coarser in size, whereas precipitate coarsening in the DP_M and DP_R alloys is significantly reduced because of the diffusion of substitutional elements that controls the coarsening mechanism.

The effect of DP steel chemistry on softening behavior is illustrated in Figure 8. The plot of the hardness difference in BM and nonisothermally tempered specimens (Figure 8(a)) suggested a trend in the extent of softening similar to that of the cementite size (Figure 5(d) through (f)) *i.e.,* DP_L (high) $\rightarrow$ DP_M $\rightarrow$ DP_R (low). The normalized softening (Figure 8(b)) suggested that DP steel of rich chemistry has a higher resistance to softening in nonisothermal tempering,[1] which was supported well by previous studies on the

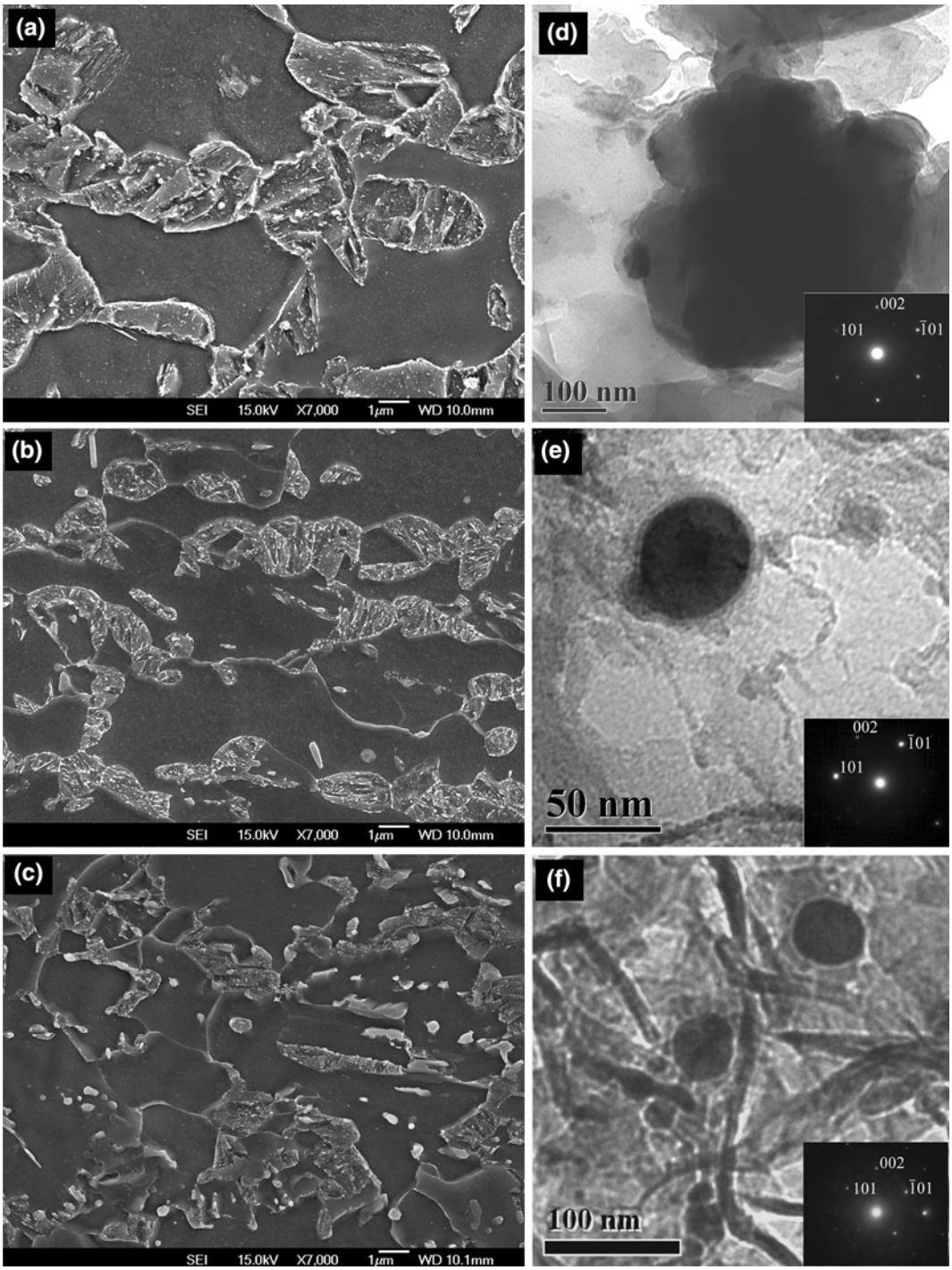

Fig. 5—SEM micrographs showing nonisothermally tempered martensite in (*a*) DP_L, (*b*) DP_M, and (*c*) DP_R. The representative extracted carbides and corresponding SAD pattern in the inset image confirming the $[010]_\theta$ zone axis of cementite from (*d*) DP_L, (*e*) DP_M, and (*f*) DP_R steels recorded with a camera length of 770 mm, 530 mm, and 530 mm, respectively.

softening kinetics of DP steels subjected to nonisothermal tempering (laser welding), indicating higher resistance to softening in DP steel of richer chemistry.[3,19] The higher resistance to softening of DP_R steel was in accordance with the finer cementite (Figure 5(f)) and less decomposed structure of tempered martensite (Figure 5c); whereas a substantial drop in hardness in DP_L steel was related to the coarser cementite (Figure 5(d)) and severely decomposed tempered structure (Figure 5(a)). It may be noted also that the volume fraction of martensite in the BM was higher in DP_L steel compared with other two steels (Figure 3 and Table I), which decomposed severely during nonisothermal tempering and led to severe softening in this steel. Furthermore, the

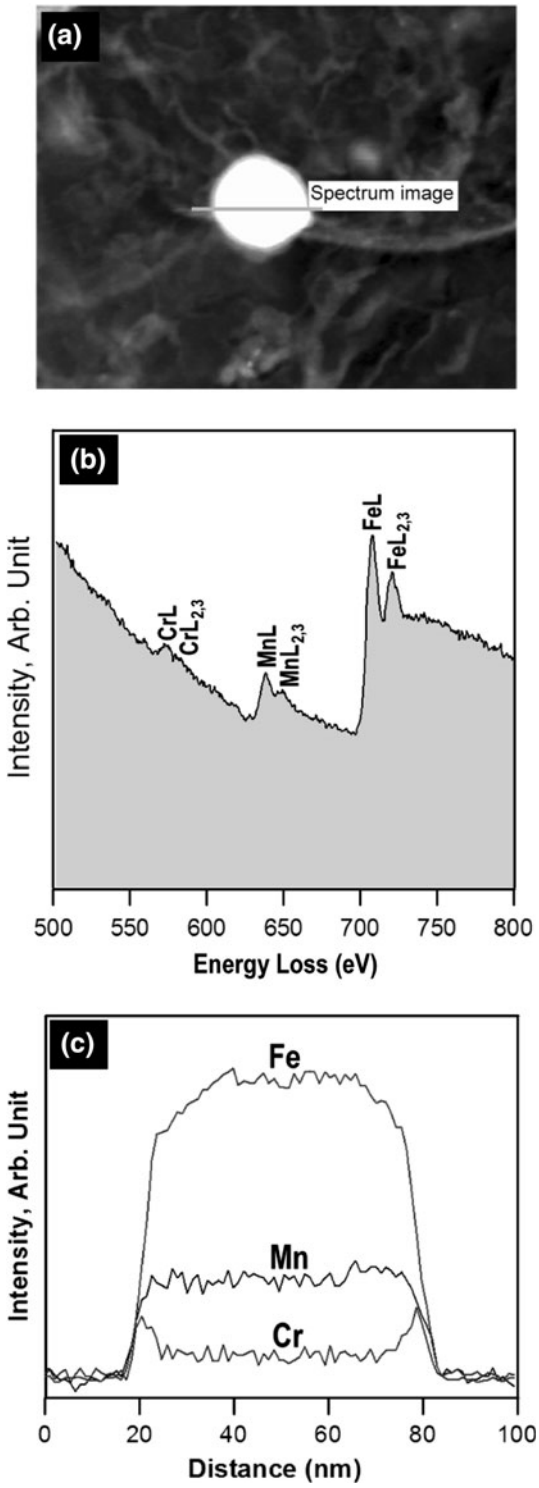

Fig. 6—Electron energy loss spectroscopy (EELS) analysis of extracted carbides from DP_M steel: (*a*) dark-field image of the analyzed cementite taken using (010) diffraction spot; (*b*) EELS spectrum indicating peaks of Fe, Mn, and Cr; and (*c*) EELS profile obtained from beam scanning across the cementite particle depicted in (a).

softening is affected strongly by the recovery process of martensite, which is controlled through the growth of cementite at lath boundaries[20] as we observed in

Table II. EDX Analysis of Precipitated Cementite in Nonisothermally Tempered DP Steels

Steel	Fe (wt pct)	Mn (wt pct)	Cr (wt pct)
DP_L	99	1	—
DP_M	74	20	6
DP_R	70	12	18

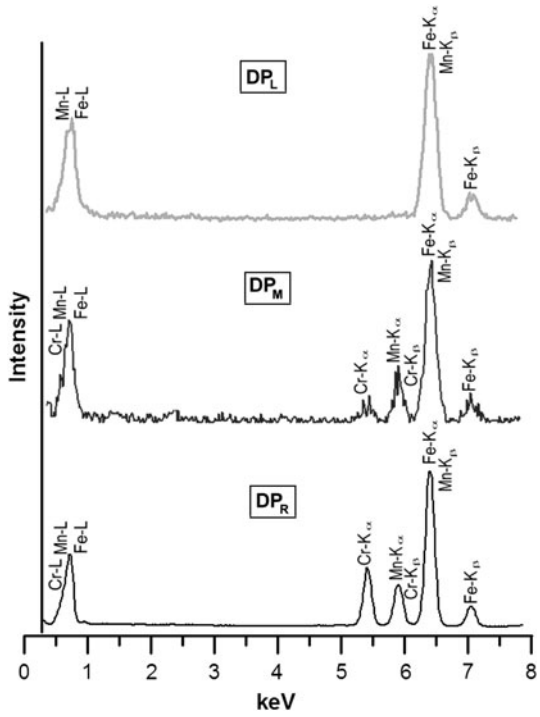

Fig. 7—EDS X-ray spectrums collected from the extracted cementite in nonisothermally tempered DP_L, DP_M, and DP_R specimens.

nonisothermal tempering of DP_M steel.[1] Thus, it was concluded that larger extent of partial recovery of α'-substructure in DP_L steel (coarser cementite) compared with that in DP_M and DP_R steels resulted in higher softening of lean chemistry DP steel subjected to nonisothermal tempering (RSW). The present work is supported by the recent studies on softening kinetics in the sub-critical heat affect zone of laser welded DP steels.[19]

We derived the following conclusions from the present study. In nonisothermal tempering, the characteristic of the tempered structure in DP steels was a function of chemistry mainly. For example, richer chemistries steels *i.e.* DP_R and DP_M formed finer cementite, 30 ± 12 nm and 45 ± 14 nm, respectively, compared with lean chemistry steel DP_L (300 ± 23 nm). The precipitated cementite in nonisothermal tempering adopts a stoichiometric form of M_3C (M = Fe, Mn, Cr) type cementite; where its substitutional content reflects the Mn and Cr levels in bulk steel chemistry. For example, nonisothermal tempering of

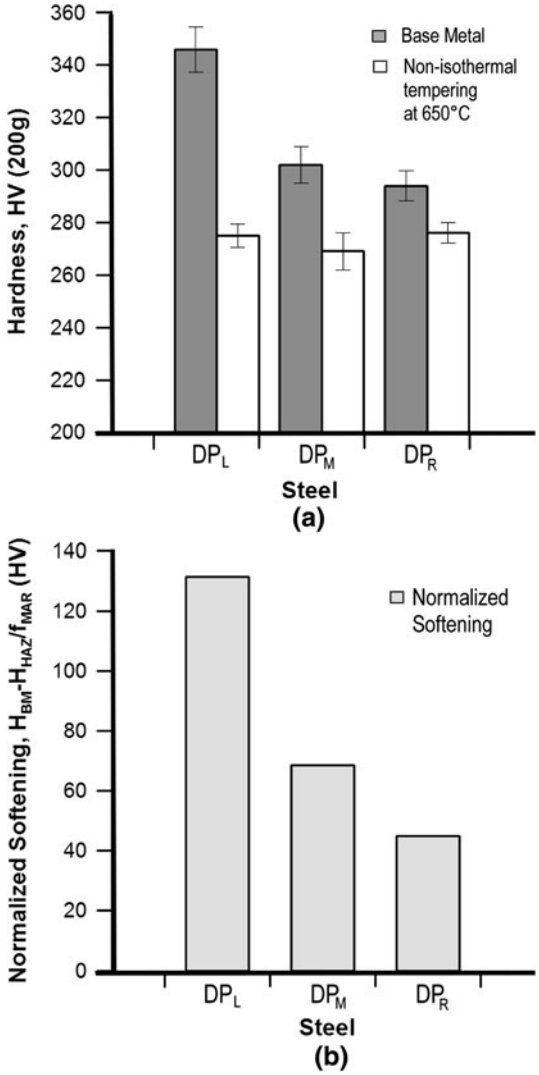

Fig. 8—Effects of chemistry on softening: (*a*) Vickers microhardness (HV) of the BM and nonisothermally tempered DP steels and (*b*) normalized softening of the DP_L, DP_M, and DP_R steels taken from Ref. 1.

DP_R steel resulted cementite with a stoichiometric form of $(Fe_{0.7}Mn_{0.12}Cr_{0.18})_3C$. The trend in extent of softening follows the trend of the cementite size: DP_L (high) → DP_M → DP_R (low).

The authors acknowledge support from Auto21 (Network of Centres for Excellence, Canada), The Initiative for Automotive Manufacturing Innovation (IAMI), ArcelorMittal Dofasco, International Zinc Association (IZA), and Huys Industries in Canada. V.H. Baltazar Hernandez acknowledges the support from CONACYT Mexico and the Autonomous University of Zacatecas Mexico.

REFERENCES

1. V.H. Baltazar Hernandez, S.S. Nayak, and Y. Zhou: *Metall. Mater. Trans. A*, 2011, vol. 42, pp. 3115–29.
2. S.K. Panda, N. Sreenivasan, M.L. Kuntz, and Y. Zhou: *J. Eng. Mater. Tech.*, 2008, vol. 130, pp. 041003-1–041003-9.
3. M. Xia, E. Biro, Z. Tian, and Y. Zhou: *ISIJ Int.*, 2008, vol. 48, pp. 809–14.
4. V.H. Baltazar Hernandez, M.L. Kuntz, M.I. Khan, and Y. Zhou: *Sci. Tech. Weld. Joining*, 2008, vol. 13, pp. 769–76.
5. V.H. Baltazar Hernandez, S.K. Panda, Y. Okita, and Y. Zhou: *J. Mater. Sci.*, 2010, vol. 45, pp. 1638–47.
6. V.H. Baltazar Hernandez, S.K. Panda, M.L. Kuntz, and Y. Zhou: *Mater. Lett.*, 2010, vol. 64, pp. 769–76.
7. M.I. Khan, M.L. Kuntz, and Y. Zhou: *Sci. Tech. Weld. Joining*, 2008, vol. 13, pp. 49–59.
8. E. Biro and A. Lee: *Sheet Metal Welding Conference XII*, AWS, Livonia, MI, 2006.
9. G.B. Olson and W.S. Owen: *Martensitic Nucleation*, ASM International, Materials Park, OH, 1992, p. 261.
10. G. Miyamoto, J.C. Oh, K. Hono, T. Furuhara, and T. Maki: *Acta Mater.*, 2007, vol. 55, pp. 5027–38.
11. J. Chance and N. Ridley: *Metall. Trans. A*, 1981, vol. 12A, pp. 1205–13.
12. N. Yurioka, H. Suzuki, S. Ohshita, and S. Saito: *Weld. J.*, 1983, vol. 62, pp. 147s–153s.
13. G. Tomas: *Metall. Trans.*, 1971, vol. 2, pp. 2373–85.
14. R.C. Thomson and M.K. Miller: *Acta Mater.*, 1998, vol. 46, pp. 2203–13.
15. P. SCAF, S. Wiesen, and U. Gonser: *Acta Mater.*, 1992, vol. 40, pp. 373–79.
16. G. Ghosh and G.B. Olson: *Acta Mater.*, 2002, vol. 50, pp. 2009–2119.
17. A. Nagao, K. Hayashi, K. Oi, S. Mitao, and N. Shikanai: *Mater. Sci. Forum*, 2007, vols. 539–543, pp. 4720–25.
18. R.C. Thomson and H.K.D.H. Bhadeshia: *Mater. Sci. Tech.*, 1994, vol. 10, pp. 205–08.
19. E. Biro, J.R. McDermid, J.D. Embury, and Y. Zhou: *Metall. Mater. Trans. A*, 2010, vol. 41A, pp. 2348–56.
20. S. Takaki, S. Iizuka, K. Tomimura, and Y. Tokunaga: *Mater. Trans. JIM*, 1991, vol. 32, pp. 207–13.